Current Optics and Photonics
Vol. 2, No. 6, December 2018, pp. 554-562
ISSN: 2508-7266(Print) / ISSN: 2508-7274(Online)
DOI: https://doi.org/10.3807/COPP.2018.2.6.554

Development of Color 3D Scanner Using Laser Structured-light Imaging Method

Youngjun Ko and Sooyeong Yi*

Department of Electrical and Information Engineering, Seoul National University of Science and Technology, Seoul 01811, Korea

(Received July 6, 2018 : revised August 24, 2018 : accepted October 12, 2018)

This study presents a color 3D scanner based on the laser structured-light imaging method that can simultaneously acquire 3D shape data and color of a target object using a single camera. The 3D data acquisition of the scanner is based on the structured-light imaging method, and the color data is obtained from a natural color image. Because both the laser image and the color image are acquired by the same camera, it is efficient to obtain the 3D data and the color data of a pixel by avoiding the complicated correspondence algorithm. In addition to the 3D data, the color data is helpful for enhancing the realism of an object model. The proposed scanner consists of two line lasers, a color camera, and a rotation table. The line lasers are deployed at either side of the camera to eliminate shadow areas of a target object. This study addresses the calibration methods for the parameters of the camera, the plane equations covered by the line lasers, and the center of the rotation table. Experimental results demonstrate the performance in terms of accurate color and 3D data acquisition in this study.

Keywords : Color 3D scanner, Rotation table, Structured-light, Line laser, Calibration
OCIS codes : (110.6880) Three-dimensional image acquisition; (100.3020) Image reconstruction-restoration; (140.3460) Lasers; (150.1488) Calibration

I. INTRODUCTION

In recent years, 3D printers have gained increasing attention for use in various applications. Small and low-priced 3D printers have become available and are spreading widely, even for personal use. Typically, a 3D printer is accompanied by a 3D scanner [1]. Manual acquisition of 3D shape data for an object is cumbersome and time-consuming; a 3D scanner makes it possible to obtain the 3D data efficiently and helps to reproduce it through a 3D printer.

There are two types of methods for 3D shape data measurement: the contact method and the non-contact method [2]. The Coordinate-Measuring-Machine is a typical example of the contact method, which uses a mechanical probe to obtain 3D shape data of an object [3]. The contact method achieves accurate measurement, but it is expensive and requires long measurement time in general. In contrast, a cost-effective and efficient measurement is possible using the non-contact method. The well-known stereo camera or the structured-light imaging method exemplifies the non-contact method, which uses photometry without direct contact with an object. Specifically, the structured-light imaging method projects a light of a distinct frequency in a structured pattern onto an object, and the 3D data is computed based on the triangulation for the distortion of the structured-light pattern, which is a function of the distance to the object [4]. Rusinkiewicz *et al*. presented a 3D scanning system using the structured-light imaging method, in which a user can rotate a target object by hand and observe a continuously-updated model to obtain a complete 3D model. They used a real-time variant of the iterative closest points (ICP) algorithm for alignment, and point-based merging and rendering algorithms [5]. In [6], a dual-camera structured-light system was developed to acquire the 3D shape of an object with high dynamic range of surface reflectivity.

The structured-light imaging method is applicable to

*Corresponding author: suylee@seoultech.ac.kr, ORCID 0000-0001-8110-1468
Color versions of one or more of the figures in this paper are available online.

various fields: reverse engineering for industrial purposes [7], restoration of cultural heritage [8, 9], biomedical applications such as 3D dental measurement [10], body shape measurement [11, 12], autonomous navigation for a mobile robot [13], object grasping and auto-calibration for manipulator robots [14, 15], etc. In [16], Levoy *et al.* presented a 3D scanning system for large statues that employs laser triangulation rangefinders, laser time-of-flight rangefinders, digital still cameras, and software for acquiring, aligning, merging, and viewing scanned data. Further progress and prospects of the structured-light imaging method for 3D data acquisition are found in [17] and [18].

A coding technique is required for the structured-light pattern generation in order to extract the points of interest in a structured-light image. Many techniques have been invented for code patterning: a simple $n \times n$ array laser beam pattern [19], color stripe pattern [8], gray code and sine wave code patterns [20], time-multiplexed pseudo-color code [21], a dual-frequency pattern combining a high-frequency sinusoid component with a unit-frequency sinusoid component [22], complementary regular and inverted patterns for high dynamic range measurement [23], and so on. In [24], an overview of various pattern codification methods including space, time, and color-coding techniques is available. An expensive digital light-processing (DLP) projector is needed for complex structured-light pattern generation and the light patterns generated by DLP are vulnerable to ambient illumination. In addition, the complex structured-light pattern requires time-consuming image processing for decoding. Tang *et al*. presented a robust pattern decoding method for shape-coded structured-light using the deep neural network technique [25]. A semiconductor laser presents an affordable alternative to the DLP projector for the structured-light because laser light is clearly distinguishable from ambient light. Zhang *et al*. developed a 3D scanning system using a handheld linear laser light and a camera [26]. Franca *et al*. used a line-type laser light for the structured-light pattern to obtain 3D point clouds at different view angles with a variable FOV camera [27].

This study presents a 3D scanner based on the laser structured-light imaging method that can acquire 3D data and color of an object simultaneously using a single camera. The color data of an object as well as the 3D data are helpful to enhance the realism of the object model. Because of the intentional illumination of the structured-light imaging method, most conventional existing structured-light imaging systems acquire 3D data only, or use an additional color camera for color data acquisition. A representative RGB-D sensor that can acquire both 3D data and color data of an object is the Kinect developed by Microsoft. The Kinect sensor also has two cameras: an infrared camera and an additional color camera [35]. The infrared camera is to obtain 3D data using the structured-light image method and the other color camera is to acquire color information from a natural visible image. Because of disparity between the two cameras, a complicated algorithm is required for matching between the two images and there are well-known limitations in the stereo correspondence such as the occlusion and the ordering problems etc.; these cause errors in the color data acquisition [36]. In contrast, this study uses a single camera to acquire a structured-light image for obtaining 3D data and a natural visible image for extracting color data. Because those images are acquired from the same camera, there is no disparity between them. Therefore, it is possible to avoid the problems in the stereo correspondence and effectively acquire both 3D data and color data without any complicated matching algorithm.

The proposed scanner system adopts two line-laser lights at either side of the camera to eliminate shadow areas of a target object. Although it seems empirically possible to reduce the shadow area by using as many laser lights as possible, there are not many studies on reduction of the shadow area in the structured-light image Experimental results demonstrate the effect of two laser lights for eliminating the shadow area in this study.

Calibration for the imaging system with the structured-light pattern is an important issue in the structured-light imaging system [28, 29]. This study also describes three-step calibration for the parameters of the camera, the line lasers, and the center of the rotation table. By taking advantage of an existing camera calibration algorithm, this study obtains the parameters for the sweep plane of the line laser and for the center of the rotation table.

Organization of this study is as follows: The overall structure of the proposed system is described in Section 2. The image processing for color and 3D data acquisition and the system calibration method are addressed in Sections 3 and 4, respectively. In Sections 5 and 6, the experimental results to verify the proposed system and concluding remarks are presented, respectively.

II. STRUCTURE OF COLOR 3D SCANNER

The color 3D scanner in this study consists of two laser lights, a color camera, and a rotation table as shown in Fig. 1. An image with a vertical line-laser light has the light pattern distorted according to the shape of a target object, and 3D data of the shape can be computed trigono-

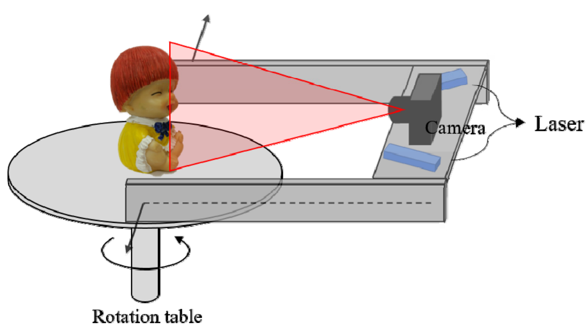

FIG. 1. Structure of color 3D scanner.

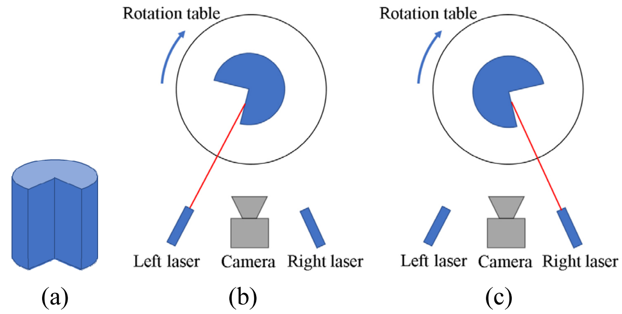

FIG. 2. Elimination of shadow area by using two laser lights. (a) Target object, (b) Shadow area of left laser light, (c) Shadow area of right laser light.

metrically from the amount of distortion and the baseline distance between the camera and the laser light source. The entire surface area of a target object is measurable by using the horizontal rotation table.

According to the shape of a target object, shadow areas may exist where the laser light image is not acquired by the camera. In order to eliminate the shadow area, two laser lights are used at either side of a camera as shown in Fig. 2. Figures 2(b) and 2(c) depict the shadow areas of the left and right laser lights at certain rotation angles of the target object. In this case, the two laser lights are complementary and it is possible to eliminate the shadow area.

III. LASER PIXEL EXTRACTION AND 3D DATA MEASUREMENT

3.1. Differential Imaging and Color Data Acquisition

The well-known differential imaging method is used to extract the laser pixels in an image in this study; the laser pixel positions are obtained by differentiating two sequential images with laser light modulation. In order to differentiate the laser pixels from the surrounding pixels in an image, an optical filter can be adopted with a camera to mitigate the influence of noise [13]. However, in that case, an additional color camera is needed to obtain the color information of a target object. Because of inevitable disparity between two cameras, this causes a certain amount of errors in the color data acquisition.

In this study, a single camera is used for both laser pixel extraction and color data acquisition. By controlling the exposure time of the image sensor, it is possible to enhance the laser pixels in the image and to obtain the color information of the extracted laser pixel positions from another natural image with the laser light off. Figure 3 shows the process of the laser pixel extraction and the color data acquisition. Figures 3(a) and 3(b) are images with the left and the right laser lights on, respectively. Those images are obtained with short exposure time of the image sensor. Figures 3(c) and 3(d) show the resultant differential images between each of the laser light images

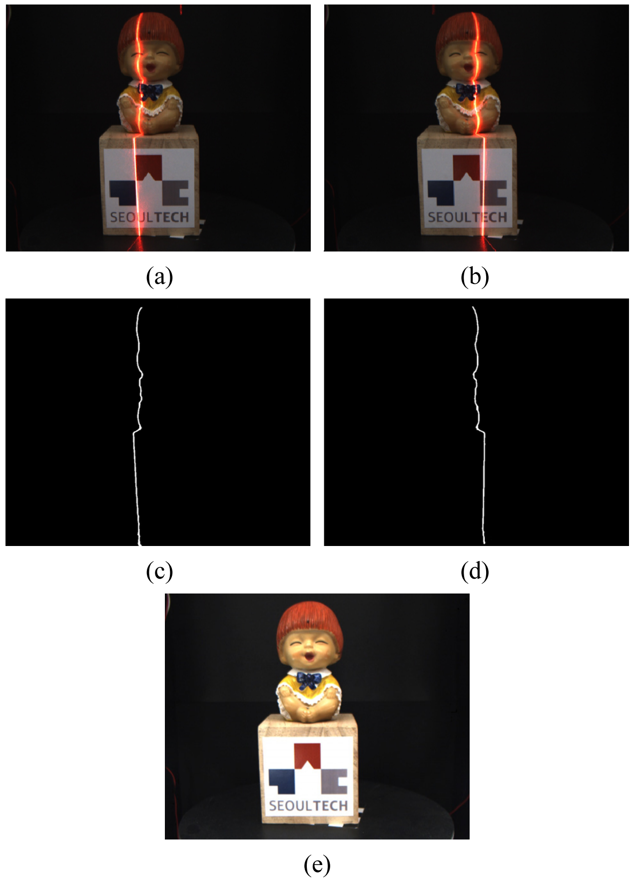

FIG. 3. Image differencing and color data acquisition. (a) Left laser-on image, (b) Right laser-on image, (c) Left differential image, (d) Right differential image, (e) Natural color image.

and an image with the laser lights off. Figure 3(e) is the natural image containing the color information with longer exposure time and the laser lights off.

3.2. Computation of 3D-coordinate Data

From the extracted laser pixel position in the image, it is possible to compute 3D data of a target object by using the transformation between the object coordinates and the image coordinates [31]. At first, it is assumed that the coordinates of the object are at the rotation center of the table for simplicity.

Figure 4 shows the transformations from the object coordinates in the real world to the pixel coordinates in the image sensor. Each of the transformations in the homogeneous coordinate representation is calculated as follows:

1) The geometric transformation between the object coordinates and the camera coordinates:

$$P_c = T_g \cdot P_w, \qquad T_g = \begin{bmatrix} R_{3\times3} & T_{3\times1} \\ 0_{3\times1} & 1 \end{bmatrix} \tag{1}$$

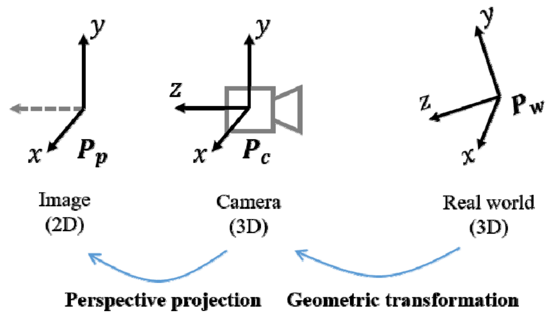

FIG. 4. Image coordinate transformation.

2) The perspective transformation from the camera coordinates to the image coordinates:

$$P_p = \frac{1}{z_c} T_p \cdot P_c, \quad T_p = \begin{bmatrix} f_x & 0 & c_x & 0 \\ 0 & f_y & c_y & 0 \\ 0 & 0 & 1 & 0 \end{bmatrix} \tag{2}$$

The symbols in Eqs. (1) and (2) are summarized as

- $P_w = \begin{bmatrix} x_w & y_w & z_w & 1 \end{bmatrix}^t$: A point in the object coordinates.
- $P_c = \begin{bmatrix} x_c & y_c & z_c & 1 \end{bmatrix}^t$: A point in the camera coordinates.
- $P_p = \begin{bmatrix} x_p & y_p & 1 \end{bmatrix}^t$: A point in the image coordinates.
- T_g: The homogeneous transformation including rotation $R_{3\times3}$ and translation $T_{3\times1}$.
- f_x and f_y: The focal length of a camera lens.
- c_x and c_y: The optical axis of a camera lens.

The composition of Eqs. (1) and (2) is obtained as Eq. (3).

$$P_p = T_{3\times4} \cdot P_w \quad \equiv \quad \begin{bmatrix} x_p \\ y_p \\ 1 \end{bmatrix} = T_{3\times4} \cdot \begin{bmatrix} x_w \\ y_w \\ z_w \\ 1 \end{bmatrix} \tag{3}$$

where $T_{3\times4} = T_p \cdot T_g$. Eq. (4) is rewritten as Eq. (4),

$$\begin{bmatrix} x_p t_{31} - t_{11} & x_p t_{32} - t_{12} & x_p t_{33} - t_{13} & x_p t_{34} - t_{14} \\ y_p t_{31} - t_{21} & y_p t_{32} - t_{22} & y_p t_{33} - t_{23} & y_p t_{34} - t_{24} \\ 0 & 0 & 0 & 0 \end{bmatrix} \begin{bmatrix} x_w \\ y_w \\ z_w \\ 1 \end{bmatrix} = \mathbf{0} \tag{4}$$

where t_{ij}, $1 \le i \le 3$, $1 \le j \le 4$ represents the elements of the composite transformation $T_{3\times4}$ in Eq. (3).

Another condition to uniquely determine a point (x_w, y_w, z_w) in the object coordinates from the image measurement (x_p, y_p) is obtained from the plane equation of the line-laser light. Because the line-laser light covers a plane in 3D space, the target points on the object are placed on the plane Eq. (5).

$$c_1 x_w + c_2 y_w + c_3 z_w + 1 = 0 \tag{5}$$

Combination of Eqs. (4) and (5) yields the following for computing 3D coordinate data (x_w, y_w, z_w) of an object from the extracted laser pixel position (x_p, y_p) in the image.

$$\begin{bmatrix} x_p t_{31} - t_{11} & x_p t_{32} - t_{12} & x_p t_{33} - t_{13} & x_p t_{34} - t_{14} \\ y_p t_{31} - t_{21} & y_p t_{32} - t_{22} & y_p t_{33} - t_{23} & y_p t_{34} - t_{24} \\ c_1 & c_2 & c_3 & 1 \end{bmatrix} \begin{bmatrix} x_w \\ y_w \\ z_w \\ 1 \end{bmatrix} = \mathbf{0}$$

$$\equiv \begin{bmatrix} x_w \\ y_w \\ z_w \end{bmatrix} = \begin{bmatrix} x_p t_{31} - t_{11} & x_p t_{32} - t_{12} & x_p t_{33} - t_{13} \\ y_p t_{31} - t_{21} & y_p t_{32} - t_{22} & y_p t_{33} - t_{23} \\ c_1 & c_2 & c_3 \end{bmatrix}^{-1} \begin{bmatrix} -x_p t_{34} + t_{14} \\ -y_p t_{34} + t_{24} \\ -1 \end{bmatrix} \tag{6}$$

Because the 3D data, (x_{wi}, y_{wi}, z_{wi}), is represented in the object coordinates, it should be transformed into the coordinates at the rotation center and then, transformed again by taking the table rotation into account. Consequently, 3D data of an object in the fixed reference coordinates is given as follows:

$$\begin{bmatrix} x_{oi} \\ y_{oi} \\ z_{oi} \\ 1 \end{bmatrix} = \begin{bmatrix} \cos\theta_i & -\sin\theta_i & 0 & 0 \\ \sin\theta_i & \cos\theta_i & 0 & 0 \\ 0 & 0 & 1 & 0 \\ 0 & 0 & 0 & 1 \end{bmatrix} \begin{bmatrix} x_{wi} - x_r \\ y_{wi} - y_r \\ z_{wi} \\ 1 \end{bmatrix} \tag{7}$$

where (x_r, y_r) represents the coordinate value of the rotation center in the object coordinates, $0° \le \theta_i \le 360°$ denotes the rotation angle, and the subscript i represents the index of the rotation.

IV. SYSTEM CALIBRATION

In order to obtain the 3D data of an object, the system parameters of the camera transformation, the sweep plane of the laser, and the center of the rotation table should be known. This study proposes a three-step algorithm by taking advantage of an existing camera calibration method.

It is well-known that a lens of a camera has distortions and it should be corrected for the measurement accuracy. In general, the lens distortion decreases as the FOV (Field of View) becomes narrower. Because the scanner in this study measures an object on a 360° rotation table, it is better to use a lens with narrow FOV. Because the camera lens adopted in this study has 20° narrow FOV, its distortion is small enough to be neglected in this study.

4.1. Step 1: Calibration for t_{ij}, $1 \le i \le 3$, $1 \le j \le 4$

The camera calibration algorithm proposed in [32] is briefly introduced in this study. Eq. (3) implies that the vectors P_p and $T_{3\times4} \cdot P_w$ are collinear. Their vector product is $P_p \times (T \cdot P_w) = \mathbf{0}_{3\times1}$, and the expanded form is

$$\begin{bmatrix} \mathbf{0}_{4\times1}{}^t & -P_w{}^t & y_p P_w{}^t \\ P_w{}^t & \mathbf{0}_{4\times1}{}^t & -x_p P_w{}^t \\ -y_p P_w{}^t & x_p P_w{}^t & \mathbf{0}_{4\times1}{}^t \end{bmatrix} \begin{bmatrix} T_1^t \\ T_2^t \\ T_3^t \end{bmatrix} = \mathbf{0}_{3\times1} \tag{8}$$

where T_1, T_2, and T_3 represent the row vectors of $T_{3\times4}$. Because Eq. (8) has only two independent conditions for the parameters in T_1, T_2, and T_3, the first two equations are selected to determine the parameters.

Given N pairs of 3D data in the object coordinates and the corresponding image points $(P_{w1}, P_{p1}), \cdots, (P_{wN}, P_{pN})$, the following augmented equations are obtained:

$$\begin{bmatrix} \mathbf{0}^t & -P_{w1}{}^t & y_{p1} P_{w1}{}^t \\ P_{w1}{}^t & \mathbf{0}^t & -x_{p1} P_{w1}{}^t \\ \vdots & \vdots & \vdots \\ \mathbf{0}^t & -P_{wN}{}^t & y_{pN} P_{wN}{}^t \\ P_{wN}{}^t & \mathbf{0}^t & -x_{pN} P_{wN}{}^t \end{bmatrix} \begin{bmatrix} T_1^t \\ T_2^t \\ T_3^t \end{bmatrix} = \mathbf{0} \quad \equiv \quad AX = \mathbf{0} \tag{9}$$

Dimensions of the matrix A are $2N \times 12$ and the solution, $\hat{X}$ of Eq. (10) is obtained as follows [32]:

$$\hat{X} = \arg\min_X \|AX\|, \qquad \|X\| = 1 \tag{10}$$

4.2. Step 2: Calibration for c_i, $1 \le i \le 3$

The object points (x_w, y_w, z_w) on the plane of the laser light satisfy Eq. (5) as described before, and are represented by the following matrix equation as

$$\begin{bmatrix} x_{w1} & y_{w1} & z_{w1} \\ x_{w2} & y_{w2} & z_{w2} \\ \vdots & \vdots & \vdots \\ x_{wN} & y_{wN} & z_{wN} \end{bmatrix} \begin{bmatrix} c_1 \\ c_2 \\ c_3 \end{bmatrix} = -\mathbf{1} \tag{11}$$

$$\equiv \quad \mathbb{P}_w \mathbf{C} = -\mathbf{1}$$

where the vector $\mathbf{1}$ denotes an N-dimensional column vector with all elements equal to 1. The solution of Eq. (11) is easily obtained as

$$\mathbf{C} = -\left(\mathbb{P}_w{}^t \mathbb{P}_w\right)^{-1} \mathbb{P}_w{}^t \mathbf{1} \tag{12}$$

4.3. Step 2: Calibration for the Rotation Center, (x_r, y_r)

A point on a rotation table draws a circle according to the rotation and the regression model of the circle on an $x-y$ surface of the table is described as

$$\begin{aligned} -2x_r x - 2y_r y + l &= -x^2 - y^2, \\ l &= x_r{}^2 + y_r{}^2 - r^2 \end{aligned} \tag{13}$$

where (x_r, y_r) denotes the rotation center and r is the radius. If a set of points, (x_{wi}, y_{wi}), on the trace of the circle are given, it is possible to obtain the rotation center as follows:

$$\begin{bmatrix} -2x_{w1} & -2y_{w1} & 1 \\ -2x_{w2} & -2y_{w2} & 1 \\ \vdots & \vdots & \vdots \\ -2x_{wN} & -2y_{wN} & 1 \end{bmatrix} \begin{bmatrix} x_r \\ y_r \\ l \end{bmatrix} = \begin{bmatrix} -x_{w1}{}^2 - y_{w1}{}^2 \\ -x_{w2}{}^2 - y_{w2}{}^2 \\ \vdots \\ -x_{wN}{}^2 - y_{wN}{}^2 \end{bmatrix} \tag{14}$$

$$\equiv \quad \mathbb{P}_w \mathbf{X}_r = \mathbf{P}$$

The pseudo-inverse solution of Eq. (15) is obtained as

$$\mathbf{X}_r = \left(\mathbb{P}_w{}^t \mathbb{P}_w\right)^{-1} \mathbb{P}_w{}^t \mathbf{P} \tag{15}$$

where $\mathbf{X}_r$ contains the parameters of the rotation center, (x_r, y_r).

V. EXPERIMENTS

5.1. Development of the Color 3D Scanner

Figure 5 shows the laser light imaging module and the scanner equipment developed in this study. Red line-laser

(a)

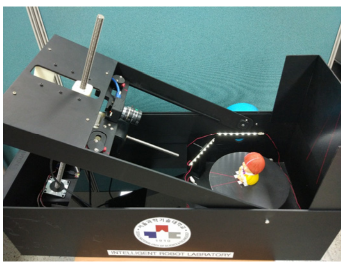

(b)

FIG. 5. Laser light imaging module and color 3D scanner. (a) Module of two line lasers and camera, (b) Scanner hardware.

sources with 660 nm wavelength and a CM3-U3-13S2C-C3 color camera are adopted. Specifications of the camera are summarized as

- Resolution: 1288 × 964 (color)
- Frame rate: 30 FPS
- Image sensor: Sony ICX445 (CCD, 1/3”)

A geared stepping motor with 0.3° step angle is used for the rotation table.

5.2. Calibration

In order to carry out the calibration in Sec. 4, a specific object with a set of known 3D coordinates is required. Figure 6 shows the calibration object with grid patterns used in this study. The size of the grid is $x = y = 10$ mm. The stepwise calibration procedure for the parameters is described as follows:

5.2.1. Step 1: Calibration for the image transformation *T*

A grid point of the calibration object in Fig. 6(a) represents $P_w = \begin{bmatrix} x_w & y_w & z_w & 1 \end{bmatrix}^t$ in the object coordinates. From the grid points $P_{w1}, \cdots, P_{wN}$ and the corresponding image points $P_{p1}, \cdots, P_{pN}$, it is possible to obtain t_{ij}, $1 \le i \le 3,\ 1 \le j \le 4$ by using Eqs. (1) and (10).

5.2.2. Step 2: Calibration for the plane equation of the line laser

Equation (4) gives two conditions to determine the 3D coordinate value (x_w, y_w, z_w) from 2D image points of the laser pixels, (x_{pi}, y_{pi}). An additional condition arises from the plane information of the laser pixels in the image. For example, in Fig. 6(b), the laser pixels in the dotted ellipse are on the $x-z$ plane in the object coordinates; the y-axis value of the corresponding 3D coordinates is $y_w = 0$. The laser pixels in the dash-dotted ellipse are on the $x-y$ plane and the z-axis value of the 3D coordinates is $z_w = 0$. Thus, by using Eq. (4) with its parameter values t_{ij} from the first step, it is possible to determine (x_w, y_w, z_w) corresponding to the laser pixel point, (x_p, y_p). The 3D coordinate values (x_{wi}, y_{wi}, z_{wi}) of all laser pixels (x_{pi}, y_{pi}), are obtained in similar fashion. Eq. (10) gives the solution for the parameters c_i, $1 \le i \le 3$.

5.2.3. Step 3: Calibration for the center of the rotation table

By rotating a grid pattern placed at an arbitrary position on the table, it is possible to acquire the overlaid image of a concentric circle with image points (x_{pi}, y_{pi}) as shown in Fig. 7. Because the grid pattern is placed on the surface of the rotation table, the object coordinate value (x_{wi}, y_{wi}, z_{wi}) has $z_{wi} = 0$. Thus, by using Eq. (4) with its parameter values t_{ij}, it is possible to determine (x_{wi}, y_{wi}, z_{wi}) corresponding to a laser pixel point (x_{pi}, y_{pi}). Note that (x_{wi}, y_{wi}, z_{wi}) is represented in the calibration object's coordinate system in Fig. 6(a) because the parameters t_{ij} obtained in Step 1 are used here. Using the points, $(x_{wi}, y_{wi}, 0)$ on the trace of a circle, the rotation center, (x_r, y_r) is obtained by Eq. (15). Figure 7(c) shows the estimation result of the rotation center in this study.

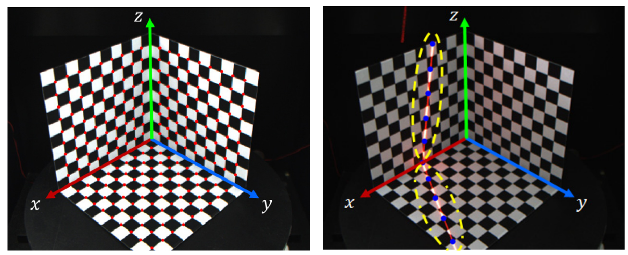

(a) (b)

FIG. 6. Calibration object. (a) Grid points, (b) Left laser points.

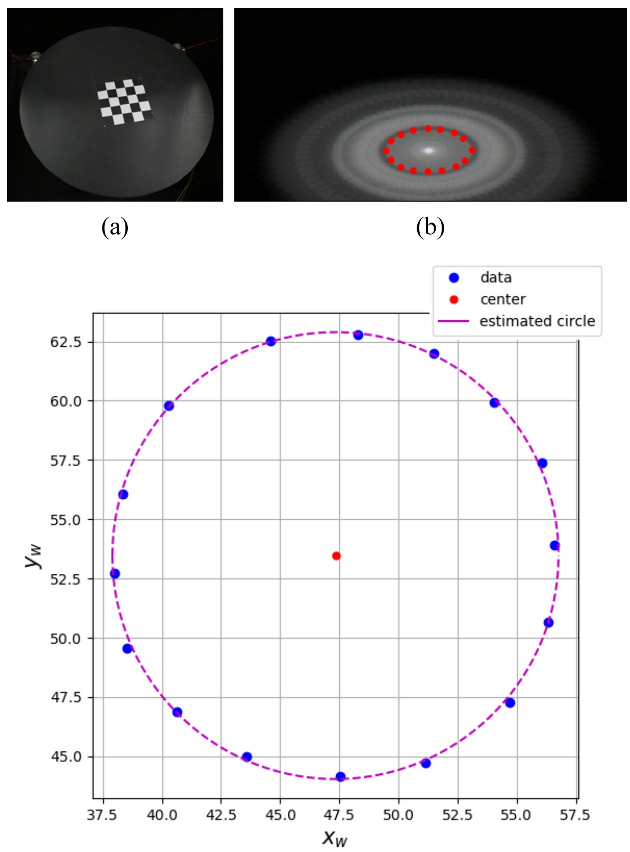

(c)

FIG. 7. Calibration for rotation center. (a) Grid pattern on rotation table, (b) Overlaid image and points on a circle, (c) Calibration result.

5.3. Accuracy

The accuracy of the 3D scan result in this study is investigated by using a planar object shown in Fig. 8(a). Figure 8(b) shows the resultant point clouds. RMS errors of the scan result are tabulated in Table 1 according to the distance between the camera and the target object. Herein, the 3D scan error is defined by the distance from a measurement point to the plane of the target object.

The accuracy of the scanner depends on the measuring distance. In this study, the goal of the measuring distance is around 300 mm. In comparison, the commercialized M&F 3D scanner developed by Matter and Form and the hand-held EVA 3D scanner by Artec 3D have approximately 0.25 mm and 0.1 mm accuracies, respectively [33, 34]. Those scanners are incapable of color data acquisition.

5.4. Elimination of Shadow Areas

Figure 9 demonstrates the elimination of shadow areas by using two laser lights. Figures 9(b) and 9(c) show the existence of some shadow areas when only one laser light is used. In contrasts, the entire target object is covered using two complementary lasers as shown in Fig. 9(d).

5.5. Result of Scan

Figures 10 and 11 show the results of scans for real objects: a white plaster and a color doll. The photo of the target objects are shown in Figs. 10(a) and 11(a), respectively. Figures 10(b) and 11(b) are the point clouds of the objects from the scanner. A point in the clouds contains 3D coordinates as well as color information. A planar white LED light with intensity of 470 lux is used for the natural image acquisition. Figures 10(c) and 11(c) show the Poisson surface reconstructions from the point clouds by using the open source MeshLab [30].

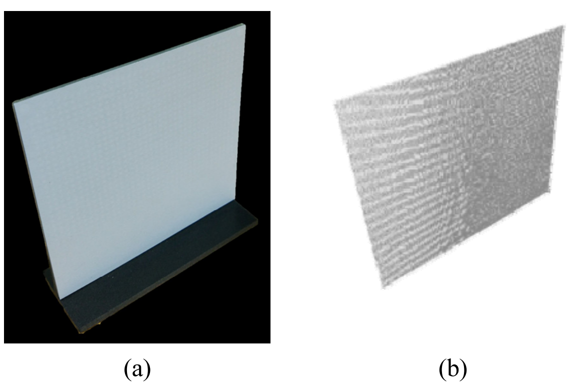

FIG. 8. 3D scan of planar object. (a) Planar object (photo), (b) Result of scan.

TABLE 1. RMS errors according to object distance

Distance (mm)	270	280	290	300	310
RMS error (mm)	0.1122	0.1318	0.1411	0.1787	0.1870

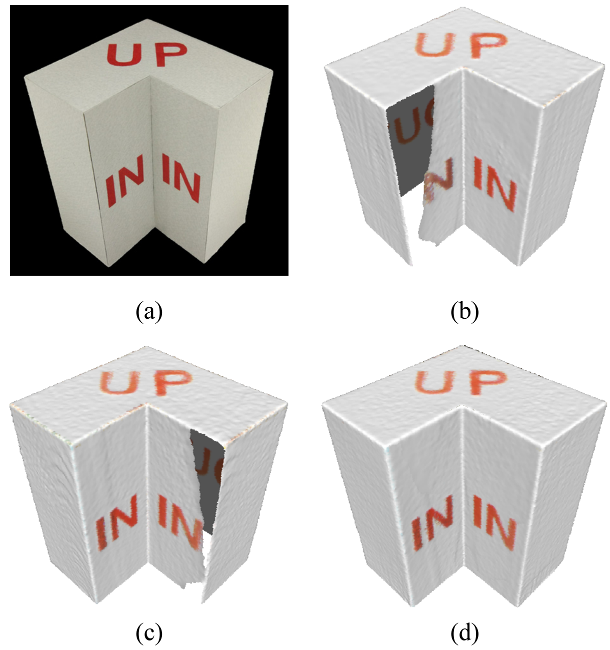

FIG. 9. Elimination of shadow areas. (a) Object (photo), (b) Scan result by the right laser, (c) Scan result by the left laser, (d) Result using both scans.

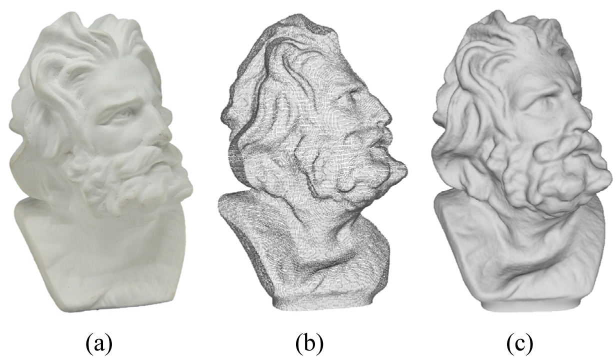

FIG. 10. Result of scan: A white plaster. (a) Object (photo), (b) 3D point cloud, (c) Poisson surface reconstruction.

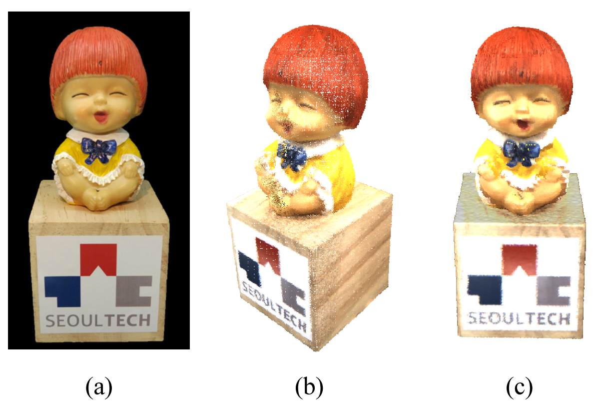

FIG. 11. Result of scan: A color doll. (a) Object (photo), (b) 3D point cloud, (c) Poisson surface reconstruction.

VI. CONCLUSION

In this study, a color 3D scanner is presented that can acquire 3D shape data and color data of a target object simultaneously based on the structured-light imaging method. The scanner consists of a color camera, two line lasers, and a rotation table. The rotation table makes it possible to scan the entire surface of an object and the two complementary line-laser lights assist in eliminating any shadow areas of the object. By modulating the laser lights, it is possible to obtain both the 3D data and color data of an object with a single camera. The color data enhances the realism of the 3D object model. Because the proposed system uses simple line-laser lights and a single camera, effective and fast image processing is possible. A three-step calibration method is used for the camera parameters, the plane equation of the line-laser light, and the center of the rotation table. Experimental results demonstrate the performance of the proposed scanner in terms of color and 3D data acquisition. The main contributions of this study are summarized as 1) a color 3D scanner using a single camera, 2) analysis on the elimination of shadow area in the structured-light image, and 3) the three-step calibration algorithm for the scanner system.

ACKNOWLEDGMENT

This study was supported by the Research Program funded by the SeoulTech (Seoul National University of Science and Technology).

REFERENCES

1. L. Zhang, H. Dong, and A. Saddik, "From 3D sensing to printing: a survey," ACM Trans. Multimedia Comput., Commun., Appl. **12**, 1-24 (2016).
2. J. Beraldin, F. Blais, L. Cournoyer, G. Godin, and M. Rioux, "Active 3D sensing," NRC Tech. Rep. **44159**, Ottawa (2000).
3. A. Weckenmann. G. Peggs, and J. Hoffmann, "Probing systems for dimensional micro- and nano-metrology," Meas. Sci. Technol. **17**, 504-509 (2006).
4. R. Jain, R. Kasturi, and B. G. Schunck, Machine vision, McGraw-Hill (1995).
5. S. Rusinkiewicz, O. Hall-Holt, and M. Levoy, "Real-time 3D model acquisition," SIGGRAPH (2002).
6. G. Liu, X. Liu, and Q. Feng, "3D shape measurement of objects with high dynamic range of surface reflectivity," Appl. Opt. **50**, 4557-4565 (2011).
7. F. Buonamici, M. Carfagni, and Y. Volpe, "Recent strategies for 3D reconstruction using reverse engineering: a bird's eye view," Adv. Mech., Des. Eng. Manuf. 841-850 (2017).
8. C. Rocchini, P. Cignoni, C. Montani, P. Pingi, and R. Scopigno, "A low cost 3D scanner based on structured light," Comput. Graphics Forum **20**, 299-308 (2001).
9. G. Pavlidis, A. Koutsoudis, F. Arnaoutoglou, V. Tsioukas, and C. Chamzas, "Methods for 3D digitization of cultural heritage," J. Cult. Heritage **8**, 93-98 (2007).
10. L. Chen and C. Huang, "Miniaturized 3D surface profilometer using digital fringe projection," Meas. Sci. Technol. **16**, 1061-1068 (2005).
11. J. Sturm, E. Bylow, F. Kahl, and D. Cremers, "CopyMe3D: scanning and printing persons in 3D," in *Proc. of German Conference on Pattern Recognition* (Germany, Sept. 2013), pp. 405-414.
12. F. Lilley, M. Lalor, and D. Burton, "Robust fringe analysis system for human body shape measurement," Opt. Eng. **39**, 187-195 (2000).
13. J. Moigne and A. Waxman, "Structured light patterns for robot mobility," IEEE J. Rob. Autom. **4**, 541-548 (1988).
14. J. Shen and N. Gans, "Robot-to-human feedback and automatic object grasping using an RGB-D camera-projector system," Robotica, Cambridge University Press (2017).
15. C. Wieghardt and B. Wagner, "Self-calibration of a mobile manipulator using structured light," in *Proc. of IEEE International Conference on Advanced Robotics (ICAR)* (China, Jul. 2017), pp. 197-203.
16. M. Levoy, K. Pulli, B. Curless, S. Rusinkiewicz, D. Koller, L. Pereira, M. Ginzton, S. Anderson, J. Davis, J. Ginsberg, J. Shade, and D. Fulk, "The digital michelangelo project: 3D scanning of large statues," in *Proc. of 27th Annual Conference on Computer Graphics and Interactive Techniques (SIGGRAPH'00)* (Jul. 2000), pp. 131-144.
17. S. Zhang, "Recent progresses on real-time 3D shape measurement using digital fringe projection techniques," Opt. Lasers. Eng. **48**, 149-158 (2010).
18. S. Gorthi and P. Rastogi, "Fringe projection techniques: Whither we are?," Opt. Lasers Eng. **48**, 133-140 (2010).
19. J. Posdamer and M. Altschuler, "Surface measurement by space encoded projected beam system," Comput. Graphics Image Process. **18**, 1-17 (1982).
20. D. Scharstein and R. Szeliski, "High accuracy stereo depth maps using structured light," in *Proc. IEEE Conference on Computer Vision and Pattern Recognition* (USA, Jun. 2003), pp. 195-202.
21. A. Boyer and P. Payeur, "Enhancing structured light range imaging by adaptation of color, exposure and focus," in *Proc. IEEE International Conference on Computational Intelligence and Virtual Environments for Measurement Systems and Applications (CIVEMSA)* (France, Jun. 2017).
22. K. Liu, Y. Wang, D. Lau, Q. Hao, and L. Hassebrook, "Dual-frequency pattern scheme for high-speed 3-D shape measurement," Opt. Express **18**, 5229-5244 (2010).
23. C. Jiang, T. Bell, and S. Zhang, "High dynamic range real-time 3D shape measurement," Opt. Express **24**, 7337 (2016).
24. J. Salvi, J. Pages, and J. Batlle, "Pattern codification strategies in structured light systems," Pattern Recognit. **37**, 827-849 (2004).
25. S. Tang, X. Zhang, Z. Song, L. Song, and H. Zeng, "Robust pattern decoding in shape-coded structured light," Opt. Lasers Eng. **96**, 50-62 (2017).
26. Z. Zhang and L. Yuan, "Building a 3D scanner system based on monocular vision," Appl. Opt. **51**, 1638-1644 (2012).
27. J. Franca, M. Gazziro, A. Ide, and J. Saito, "A 3D scanning system based on laser triangulation and variable field of view", in *Proc. IEEE International Conference on*

Image Processing (Italy, Sept. 2005), pp. 425-428.
28. O. Fleischmann and R. Koch, “Fast projector-camera calibration for interactive projection mapping,” in *Proc. of International Conference on Pattern Recognition (ICPR)* (Mexico, Dec. 2016), pp. 3798-3803.
29. S. Zhang and P. Huang, “Novel method for structured light system calibration,” Opt. Eng. **45**, 083601-083608 (2006).
30. M. Kazhdan, M. Bolitho, and H. Hoppe, “Poisson surface reconstruction,” Eurographics Symposium on Geometry Processing (2006).
31. G. Taubin and D. Moreno, “Build your own desktop 3D scanner,” SIGGRAPH2014, 28-38 (2014).
32. D. P. Bertsekas, “Constrained optimization and lagrange multiplier methods,” Academic Press, New York (2014).
33. https://matterandform.net/scanner.
34. https://www.artec3d.com/files/pdf/ArtecScanners-Booklet-EURO.pdf.
35. J. Han, L. Shao, D. Xu, and J. Shotton, “Enhanced computer vision with microsoft kinect sensor: a review,” IEEE Trans. Cybern. **43**, 1318-1334 (2013).
36. F. Alhwarin, A. Ferrein, and I. Scholl, “IR stereo kinect: improving depth images by combining structured light with IR stereo,” Lect. Notes Comput. Sci. **8862**, 409-421 (2014).